Advanced Composite Materials
Publication details, including instructions for authors and subscription information:
http://www.tandfonline.com/loi/tacm20

Damage progression analyses of transverse stitched T-joints under flexure and tensile loading

P. B. Stickler & M. Ramulu

Version of record first published: 02 Apr 2012.

To cite this article: P. B. Stickler & M. Ramulu (2006): Damage progression analyses of transverse stitched T-joints under flexure and tensile loading, Advanced Composite Materials, 15:2, 243-261

To link to this article: http://dx.doi.org/10.1163/156855106777873879

Adv. Composite Mater., Vol. 15, No. 2, pp. 243–261 (2006)

Also available online - www.vsppub.com

Damage progression analyses of transverse stitched T-joints under flexure and tensile loading *

P. B. STICKLER [1,†] and M. RAMULU [2]

[1] *The Boeing Company, P. O. Box 3707, MC: OR-CC, Seattle, WA 98124-2207, USA*
[2] *University of Washington, Department of Mechanical Engineering, Seattle, WA 98195, USA*

Received 14 October 2004; accepted 6 October 2005

Abstract—The progressive damage of a new type of composite T-joint with transverse stitching using a fiber insertion process was modeled using numerical methods. T-joints modeled herein were fabricated from dry fabric preforms using resin transfer molding. Fiber tows were inserted into the dry fabric preforms prior to consolidation. Experiments were conducted to determine the load–displacement and strain–load history under Flexure and Tensile loading. Linear, nonlinear, and damage progression finite element models were developed to predict the mechanical behavior under each load condition. Experimental observations of initial failure were marked by a discrete drop in the load–displacement behavior and the initiation and propagation of an interfacial matrix crack at the web-to-flange interface. Fiber insertion bridging and fiber insertion breakage were observed at T-joint ultimate failure. The linear and nonlinear analyses show good correlation with experimental results through T-joint initial failure. An effective stress failure criterion was applied to predict damage initiation at the T-joint web-to-flange interface. The damage progression finite element analyses showed good agreement with experimentally determined load–displacement values through ultimate failure. The predictive models developed herein are used in future parametric design studies.

Keywords: T-joints; damage mechanics; numerical analysis; mechanical testing.

1. INTRODUCTION

Composite materials are being used extensively in load-bearing applications throughout the aerospace industry. One potential weakness of composite materials is their poor out-of-plane load transfer capability. A method of improving the out-of-plane performance of composite materials is through design optimization using finite element analysis (FEA). Numerical methods have been employed

*Edited by the JSCM.

†To whom correspondence should be addressed. E-mail: patrick.b.stickler@boeing.com

to (1) evaluate the mechanical behavior of integral composite joints and (2) optimize the out-of-plane load transfer capability. Gillespie and Pipes [1] evaluated integral composite joints using two-dimensional linear elastic FEA and experimentation. Integral joints in aircraft wing boxes were modeled and experiments were conducted for the cases of no-insert, a titanium insert, and a graphite epoxy insert. A bilinear load–displacement response was observed for the cases of titanium and graphite inserts; good agreement was shown between numerically predicted and experimentally determined responses. Another method of improving the out-of-plane performance of composite joints is through the use of transverse stitching or z-fiber insertions. Transverse stitching is a two-sided continuous stitching process using either fiber yarn or tow. Z-fibers, on the other hand, are discrete pins placed through-the-thickness of a laminate or joint to provide z-directional reinforcement. Analytical and numerical evaluations of single lap joints with transverse stitching have been performed [2, 3]. In these investigations, the effects of stitch parameters on joint failure were evaluated. Transverse stitching was shown to reduce the critical peel stress when stitches were located near the specimen edge; increasing the stitch modulus was shown to reduce critical peel stresses. The mechanics of z-fiber reinforcements were studied and it was found that the presence of z-fibers at the interface reduced the crack tip nodal stress [4].

However, failure of composite materials with applied out-of-plane loads tends to be matrix dominated in T-joints under flexure and tensile loading, producing out-of-plane loading of the flange member. The modeling of structures with this type of loading requires consideration of material and geometric nonlinearities. Jones and Alesi analyzed T-stiffeners with out-of-plane loading using FEA [5] with material and geometric nonlinearities. Experimental and numerical results showed good correlation with the inclusion of nonlinear effects. Matrix dominated failures in composite joints were also studied [6]. Progressive damage of composite T-joints was studied extensively by Phillips and Shenoi [7]. In their study, it was shown that T-joints fail in a series of steps with increasing applied load. A progressive FEA was performed to model the damage evolution through ultimate failure. T-joints were shown to fail by delamination in the corner plies and matrix cracking at the web-to-flange interface. Another study used an iterative process to evaluate T-joints with viscoelastic inserts [8].

In order to understand the failure mechanisms associated with transversely stitched T-joints under flexure and tension loading, a finite element analysis was conducted. A brief review of our experimental observations of failure is given in this paper. These observations were incorporated into the finite element model. In the present analysis, T-joints with transverse stitching are modeled through ultimate failure for the first time under flexure and tensile loading. A nonlinear FEA, including both material and geometric nonlinearities, was developed to model the behavior through initial failure. T-joints were modeled through ultimate failure using a progressive damage FEA.

2. EXPERIMENTAL OBSERVATIONS

A new one-sided stitching process, referred to as fiber insertion, was developed as a low-cost method of joining two-dimensional dry fiber preforms. A typical T-joint is shown in Fig. 1a. Figure 1b shown the T-joint configuration for both flexure and tensile loading. Specimens are fabricated from T-300 dry fabric preforms. Transverse stitching is accomplished using IM7 6K fiber tow insertions and specimens are consolidated using PR500 toughened epoxy resin and the RTM process.

Extensive experimental investigations were performed on T-joints constructed using the fiber-insertion process under flexure, tensile and shear loading [9–12]. In these experiments, T-joints with transverse stitching failed in a series of steps with increased load. Figure 1c shows a typical failed T-joint specimen. Post-failure analysis revealed that damage initiated in the fillet region at the web-to-flange interface. Increased load beyond initial failure caused crack propagation in the fillet region and across the web-to-flange interface. Additional loading caused fiber insertion bridging, leading to ultimate T-joint failure via fiber-insertion breakage and pullout. T-joint flexure and tension specimen web and flange members remained partially intact through ultimate failure. Shear specimens failed with complete separation of the web and flange. T-joints were modeled up to initial failure using linear elastic finite element analysis. Predicted and experimental results showed good agreement in this load range. However, these investigations did not included progressive damage analyses, representing the entire load history. In the present analysis, T-joints are modeled in a series of steps representing accumulated damage through ultimate failure.

3. FINITE ELEMENT MODELS AND METHOD OF ANALYSIS

Linear, nonlinear, and progressive damage analyses were performed on the T-joint under flexure and tensile loading using ANSYS FEA software [13]. Two-dimensional finite element models were created using a plane strain assumption. Plane strain was assumed in this case because the specimen width is much greater than the web or flange thickness. Fiber insertion tows were modeled using simple beam elements. Damage progression was modeled in a series of discrete steps representing an accumulation of damage under increased load.

3.1. Finite element model

Table 1 shows the material properties used in the finite element analysis. Vendor-supplied properties were used for the Hexcel IM7 fiber insertions and 3M PR520 resin [14, 15]. The experimentally determined elastic laminate properties, as developed previously, were used for the T-300/PR520 quasi-isotropic web and flange [16]. A nonlinear analysis was performed using both nonlinear elastic

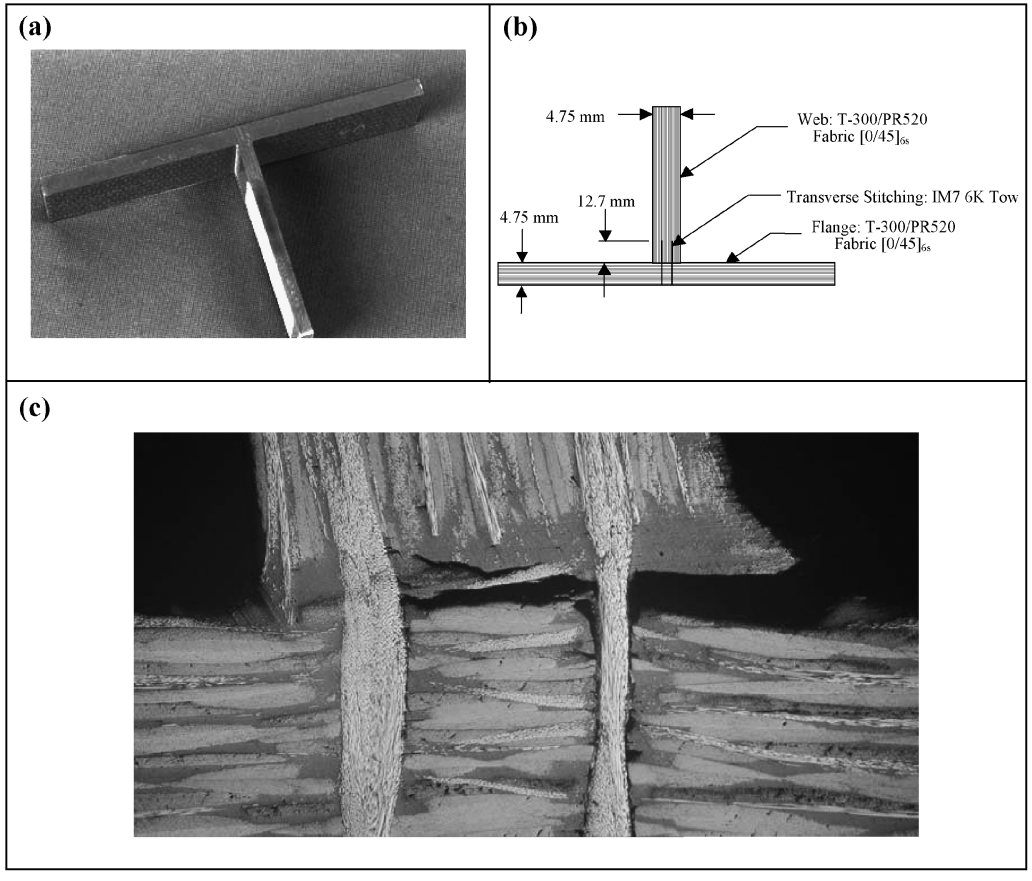

Figure 1. Transverse stitched composite T-joint: (a) typical as fabricated specimen, (b) flexure and tension specimen configuration, and (c) a typical failed specimen.

Table 1.
T-joint constituent elastic material properties (global coordinate system)

Property	Region 1 (IM7 Fiber Insertion)	Region 2 (PR520 Resin)	Region 3 (T-300/PR520 Web)	Region 4 (T-300/PR520 Flange)
E_{11} (GPa)	276	3.54	44.24	9.73
E_{22} (GPa)	276	3.54	9.73	44.24
E_{33} (GPa)	276	3.54	44.24	44.24
ν_{12}	0.30	0.38	0.37	0.37
ν_{23}	0.30	0.38	0.37	0.31
ν_{13}	0.30	0.38	0.31	0.37
G_{12} (GPa)	106	1.28	2.98	2.98
G_{23} (GPa)	106	1.28	2.98	16.53
G_{13} (GPa)	106	1.28	16.53	2.98

Table 2.
Nonlinear PR520 neat resin properties

Stress (MPa)	Strain (%)	Strain	E (GPa)	True stress (MPa)	True strain
0.00	0.000	0.0000	0.000	0.00	0.0000
20.68	0.590	0.0059	3.506	20.81	0.0059
41.37	1.300	0.0130	3.182	41.91	0.0129
62.05	2.200	0.0220	2.821	63.42	0.0218
82.74	3.500	0.0350	2.364	85.63	0.0344
91.01	6.020	0.0602	1.512	96.49	0.0585

material properties for the resin-rich interface region and large displacement. Nonlinear material properties were incorporated using the ANSYS multilinear kinematic hardening (KINH) function. Table 2 shows the PR520 stress-strain data input for the neat resin. The true-stress and true-strain data were input directly into the KINH function table. A built-in Newton-Raphson iterative procedure was used to solve each incremental load step of the nonlinear analysis.

The IM7 6k fiber tow cross-sectional area, A_{tow} was determined using the following expression:

$$A_{\text{tow}} = \left(\frac{\pi d_{\text{f}}^2}{4}\right) * (\text{number of \# filaments})$$

where d_{f} is the filament diameter [17]. There are 6000 filaments per 6k tow and 2 tows per fiber insertion. The IM7 fibers have a filament diameter of 5 μm and a fiber tow area of 0.15 mm. The nominal circular tow diameter was determined to be 0.50 mm, assuming a packing fraction of 0.75, where the packing factor is the area of fibers divided by the area of a circle. The fiber insertion tow area and diameter were used as input to the finite element model (FEM) element attributes.

In order to numerically model the T-joint, the resin-rich interface zone thickness was required. Based on specimen optical micrographs, the nominal resin-rich

Table 3.
Finite element analysis model attributes

Attribute	Flexure	Tension
Model type	2D Linear elastic, nonlinear elastic, and damage progression Plane strain	2D Linear elastic and damage progression Plane strain
ANSYS Element	LINK1 — 2D spar PLANE2 — 2D 6-node triangular structural solid PLANE183 — 2D 8-node structural solid	LINK1 — 2D spar PLANE2 — 2D 6-node triangular structural solid PLANE183 — 2D 8-node structural solid
Boundary conditions	Fixed support flange	Simple support flange

interface zone thickness was determined to be 1.25 mm. This region was assumed to be isotropic and was modeled using the PR520 neat resin properties. The variation and magnitude of the interface thickness may be attributed to preform edge roughness and fiber preform misalignment during T-joint fabrication.

The FEM, including fixed-support boundary conditions used in the flexure linear elastic, nonlinear, and progressive damage FEA is shown in Fig. 2a. Figure 2b shows the boundary conditions for the simple support tension analysis. Table 3 shows a summary of the model attributes for these analyses. The two rows of fiber insertions located in region 1 were modeled using IM7 6k fiber tow properties and 2D spar elements. Isotropic material properties were used for the resin-rich fillet and web-to-flange interface region 2. The fillet regions were modeled using 6-node triangular elements. Quasi-isotropic material properties were used for composite web and flange regions 3 and 4, respectively. The web and flange were modeled using 8-node quadrilateral elements. In the case of flexure, a nodal force was applied normal to the web 2.54 cm from the web-to-flange interface. Fixed boundary conditions (zero displacement) were assumed at the flange interface to represent the bonded flange-to-fixture attachment constraint. In the case of tension, a force was applied on the web normal to the flange representing the load frame hydraulic grips and simple support boundary conditions were applied to the flange.

3.2. Damage progression criterion

A damage progression finite element analysis was performed based on experimental observations and optical micrographs of the failed flexure specimens as reported previously [10]. These experiments demonstrated that a crack initiates from the resin-rich fillet region and traverses the web-to-flange interface under increased load. In order to model this progressive damage, a series of six step FEMs were created, representing an accumulation of damage with increased load. Figure 3a through f shows the finite element mesh for the damage progression models. In

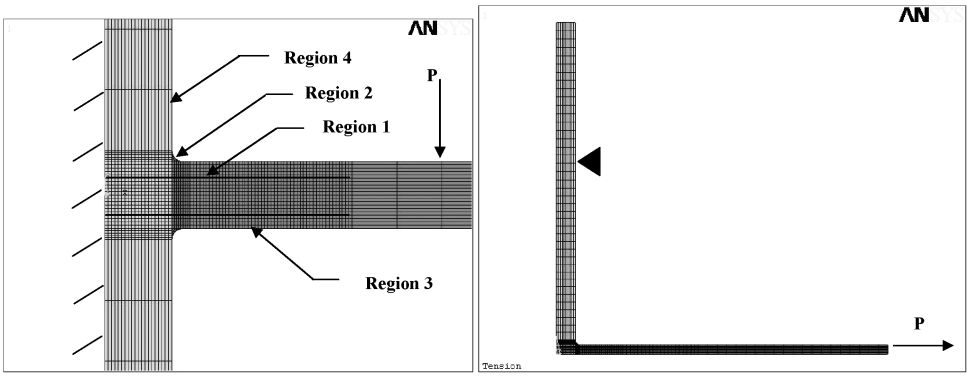

Figure 2. Finite element analysis boundary conditions and analysis regions: (a) flexure and (b) tension.

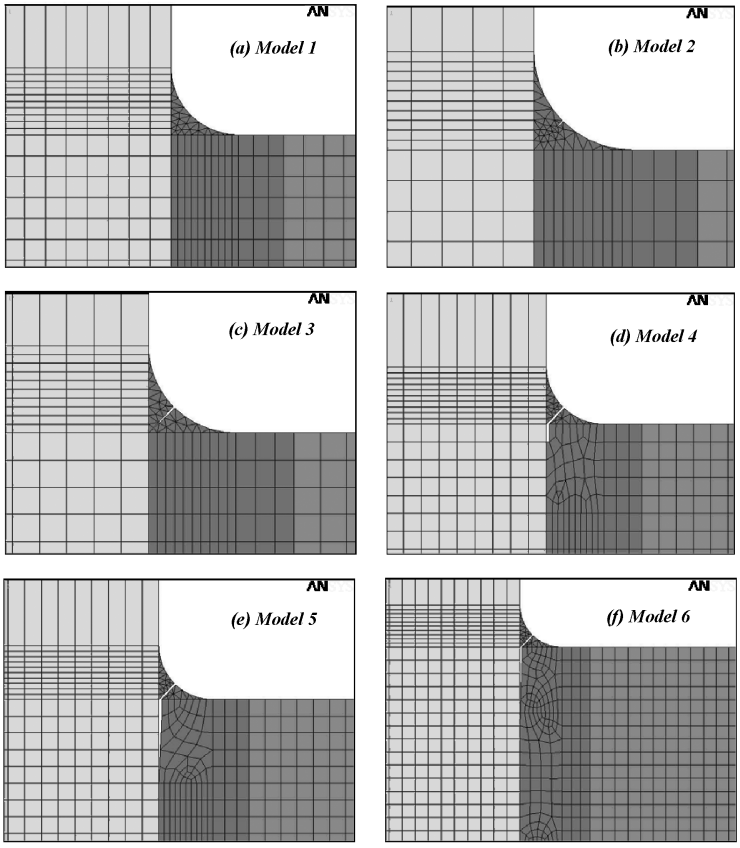

Figure 3. Flexure damage progression finite element analysis mesh for Models 1–6.

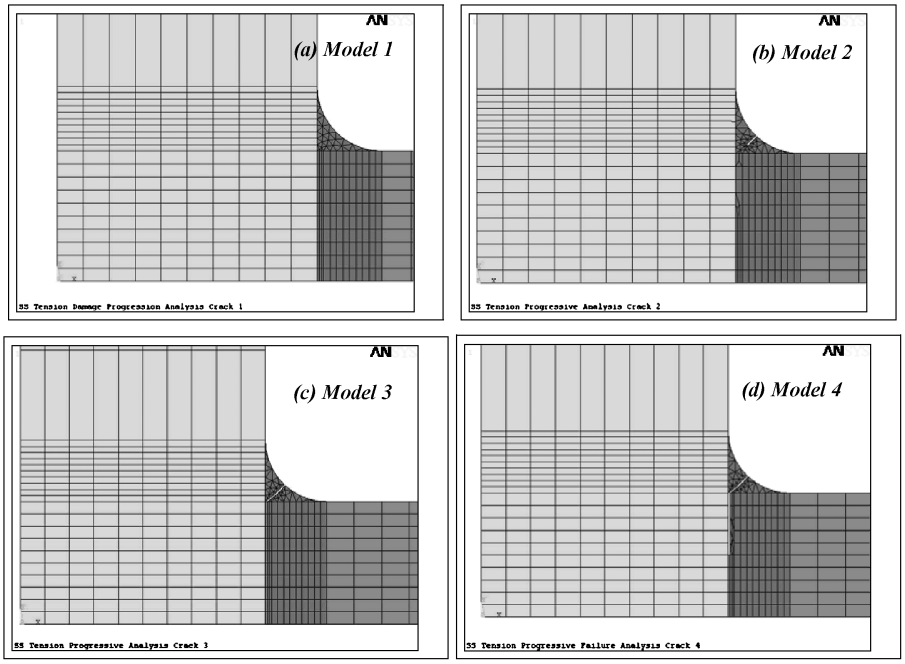

Figure 4. Tension damage progression finite element analysis mesh for Models 1–4.

Fig. 3a no damage is present, which represents the elastic region of the load–displacement record up to initial failure. Figure 3b models an incipient crack in the resin-rich fillet region at the web-to-flange interface. This represents the initial drop in load displacement. The magnitude of the drop is indicative of the extent of damage to the T-joint. Figure 3c models continued fillet crack propagation, Fig. 3d models the crack traversing the web-to-flange interface, and Fig. 3e models the crack extending to the first fiber insertion. The first fiber insertion is the insertion adjacent to the applied load. Figure 3f models the crack reaching the second fiber insertion.

A damage progression analysis was performed on the T-joint under tension loading. As in the case of the flexure numerical analysis, experimental observation of failed specimens was used in determining the extent and direction of the accumulative damage under increased load. Figure 4a through d shows the finite element mesh for the damage progression analysis. Model 1 shows the FEA mesh for the T-joint with no crack present. Model 2 represents a crack that emanates from the resin-rich radius filler. Model 3 contains a crack at the web-to-flange interface and model 4 shows the crack extending to the first IM7 fiber tow insertion.

In order to determine the extent and effect of fiber insertion degradation on T-joint deflection, an FEA was performed under constant flexural load and crack length. In this analysis, the fiber-insertion tow damage was represented by a reduction in tow area and subsequent displacement loss of T-joint stiffness. Figure 5 shows the

T-joint increases as the IM7 tow area decreases under progressive fiber insertion damage. These results were used in the damage progression analysis.

An effective stress failure criterion was used to predict the initial damage load in the T-joints. Initial T-joint damage was defined as the point when the effective stress, σ_{eff} of the constrained matrix at the web-to-flange interface exceeded the neat resin failure strength, σ_{fm}. The published failure strength of the PR520 toughened epoxy neat resin was 91.0 MPa [15].

4. RESULTS

Figures 6a and 6b show the T-joint linear and nonlinear predicted and experimental load–displacement response under flexure and tensile load, respectively. This analysis was performed using the experimentally determined initial damage load. It was noted that the experimental load–displacement plot indicates a slight amount of nonlinearity. As shown, the nonlinear analysis more closely predicts the experimental results. The numerically determined stress contour plots for the nonlinear analysis are shown in Fig. 7. The figure shows (a) local normal stress in the x-direction, (b) σ_x and in the y-direction, (c) σ_y, in-plane shear stress, τ_{xy}, and (d) the effective stress, σ_{eff}. The stress fields computed from both the linear and nonlinear analyses yielded similar results. A peak effective stress of 91.2 MPa was predicted in the linear elastic analysis. The nonlinear analysis predicts a slightly higher effective stress of 94.9 MPa at the initial damage load. As indicated, the effect stress just exceeds the neat resin tensile strength at the T-joint initial damage load. Figure 8a shows the predicted load–displacement plot under flexural load for specimen F1. Region 1 (up to initial failure) is modeled with no damage as shown in Fig. 3a. The initial crack at point 'a' coincides with a matrix crack forming in the fillet region at the web-to-flange interface and propagating to the fiber insertion adjacent to the applied load. As shown, the load–displacement plot is then nearly linear from point 'b' up to point 'c'. In this region, as indicated by the analysis, the crack is propagating to the second fiber insertion and increasing the apparent load on the first fiber insertion. From point 'c' to point 'd' in Fig. 8a, the first fiber insertion is degrading as indicated by the analysis of Fig. 4. Further loading beyond point 'd' then results in fiber tow filament breakage and insertion/matrix interface degradation.

Figure 8b shows the predicted and actual strain–load data for gage locations 9 and 12. The overall trend of the predicted response is in agreement with the experimental data. However, the predicted tensile strain at gage location 9 is approximately 26 percent higher at initial failure and 19 percent higher at ultimate failure. The predicted compressive strain at gage location 12 is approximately 13 percent lower at initial failure and 22 percent lower at ultimate failure. The difference in magnitude may potentially be attributed to T-joint web-to-flange perpendicularity tolerances during part manufacture. Figure 9 shows the effective stress contour plots for damage progression models 1 through 6. As defined by

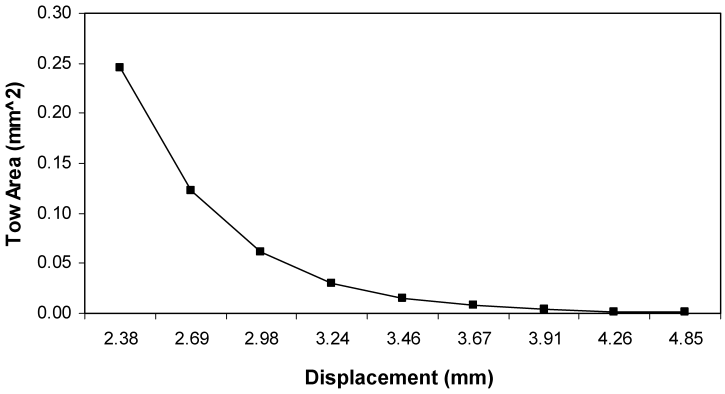

Figure 5. IM7 fiber insertion damage progression under flexure loading.

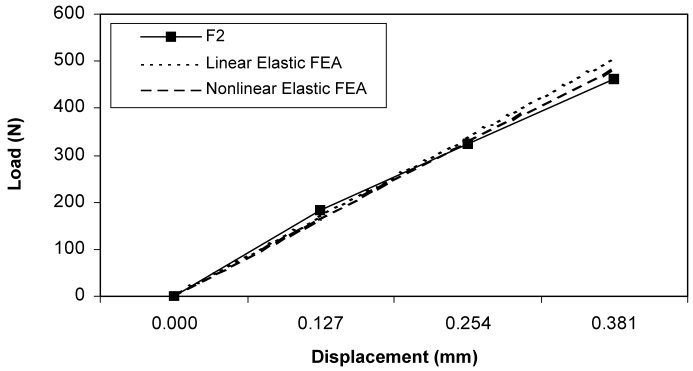

(a)

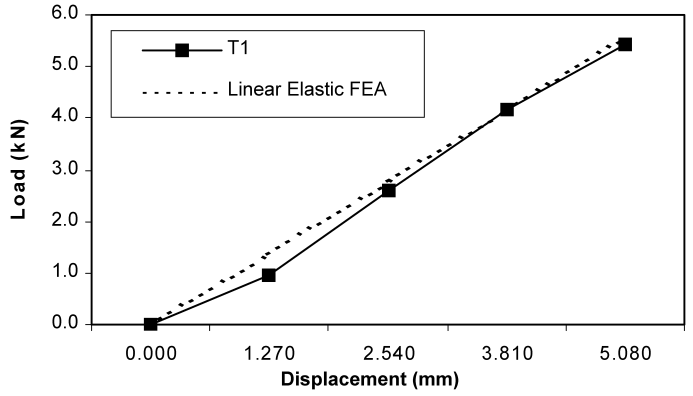

(b)

Figure 6. Predicted and actual load–displacement plot: (a) linear and nonlinear flexure specimen F2 and (b) linear elastic tension specimen T1.

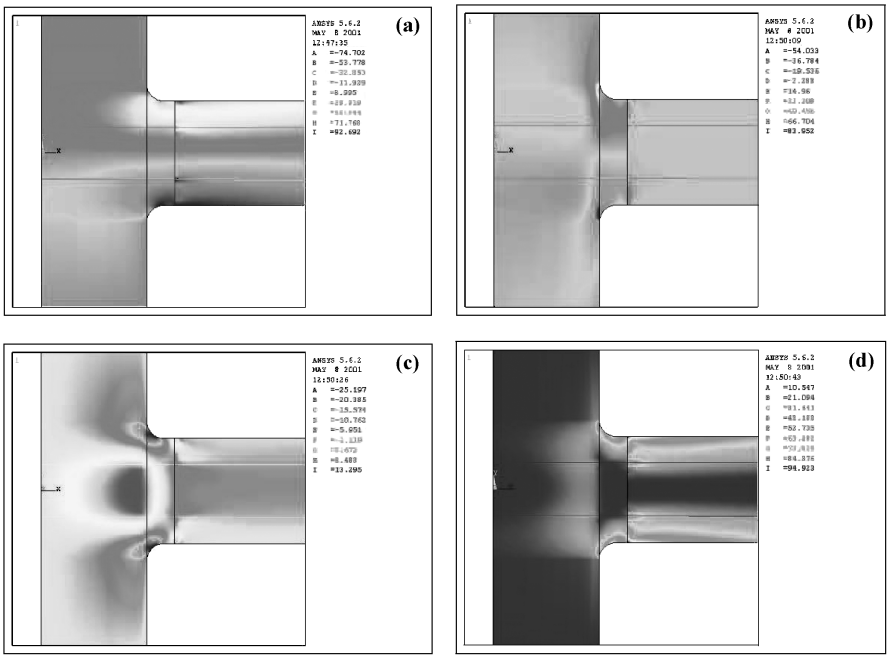

Figure 7. T-joint nonlinear elastic flexure stress contours (MPa): (a) normal stress, σ_x, (b) normal stress, σ_y, (c) in-plane shear stress, τ_{xy}, and (d) effective stress, σ_{eff}.

the failure analysis, damage progresses at the point when the peak effective stress exceeds that of the PR520 neat resin tensile strength in the radius fillet and web-to-flange interface regions. Model 6 shows the damage progressing beyond the fiber insertion adjacent to the applied load, representing extensive interfacial matrix cracking and fiber insertion bridging at the web-to-flange interface.

Figure 6b shows the predicted and actual load–displacement response of the T-joint under tension loading. Again, this analysis was performed using the experimentally determined initial damage load. Good agreement is shown between the experimental and predicted results. A damage progression analysis was performed on the T-joint under tension loading. As in the case of the flexure numerical analysis, experimental observation of failed specimens were used in determining the extent and direction of the accumulative damage under increased load. Figure 10a shows the predicted and experimental load–displacement plot through ultimate failure. At initial failure, a drop is observed in the load–displacement plot. This is indicative of initial crack formation as shown in Fig. 10a. The predicted response matches the experimental behavior. Figure 10b shows the predicted and actual strain–load response for strain gage locations 3 and 6. Close agreement is shown for predicted and experimentally determined strain at gage location 6 at T-joint ultimate failure. At gage location 3, a similar trend is shown for the predicted and actual strain response. However, strain is over-predicted by approximately 25% at ultimate failure. Variations in part

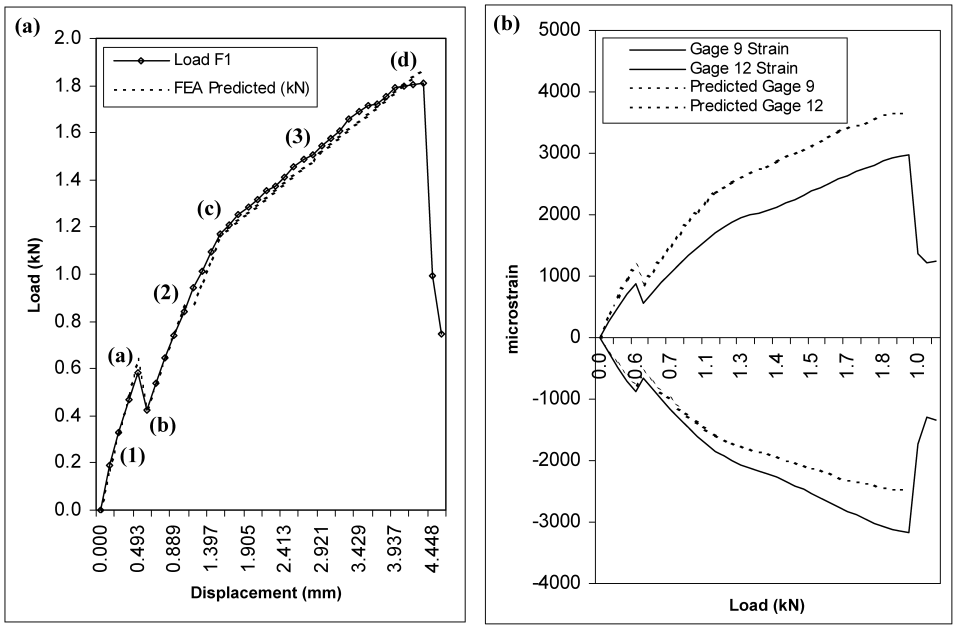

Figure 8. Damage progression under flexure loading: (a) predicted and actual load–displacement and (b) predicted and actual strain–load plot.

manufacture including web-to-flange perpendicularity, fiber insertion spacing and pitch, and preform thickness may be attributed in part to the differences in predicted and actual load–strain response. Figure 11 shows the stress contour plots for damage progression models 1 through 4 for the case of tensile loading. Again, damage progresses at the point when the peak effective stress exceeds that of the PR520 neat resin tensile strength in the radius fillet and web-to-flange interface regions.

5. DISCUSSION

5.1. Flexure analysis

The mechanical behavior of the T-300/PR520 transverse stitched composite T-joints under flexure loading may be characterized by three distinct regions as indicated on the load–displacement plot in Fig. 8a. In region 1, the behavior is nearly linear elastic up to the initial damage load, showing only a slight amount of nonlinearity near the proportional limit. In region 2, with increased load, the behavior is again nearly linear. Region 3 is marked by a change in slope of the load–displacement plot leading to catastrophic failure. The three regions of behavior are detailed in the following paragraphs.

Under initial flexure load, as represented by region 1 of the load–displacement plot of Fig. 8a, the T-joint web deflects under increased load. This has the effect of

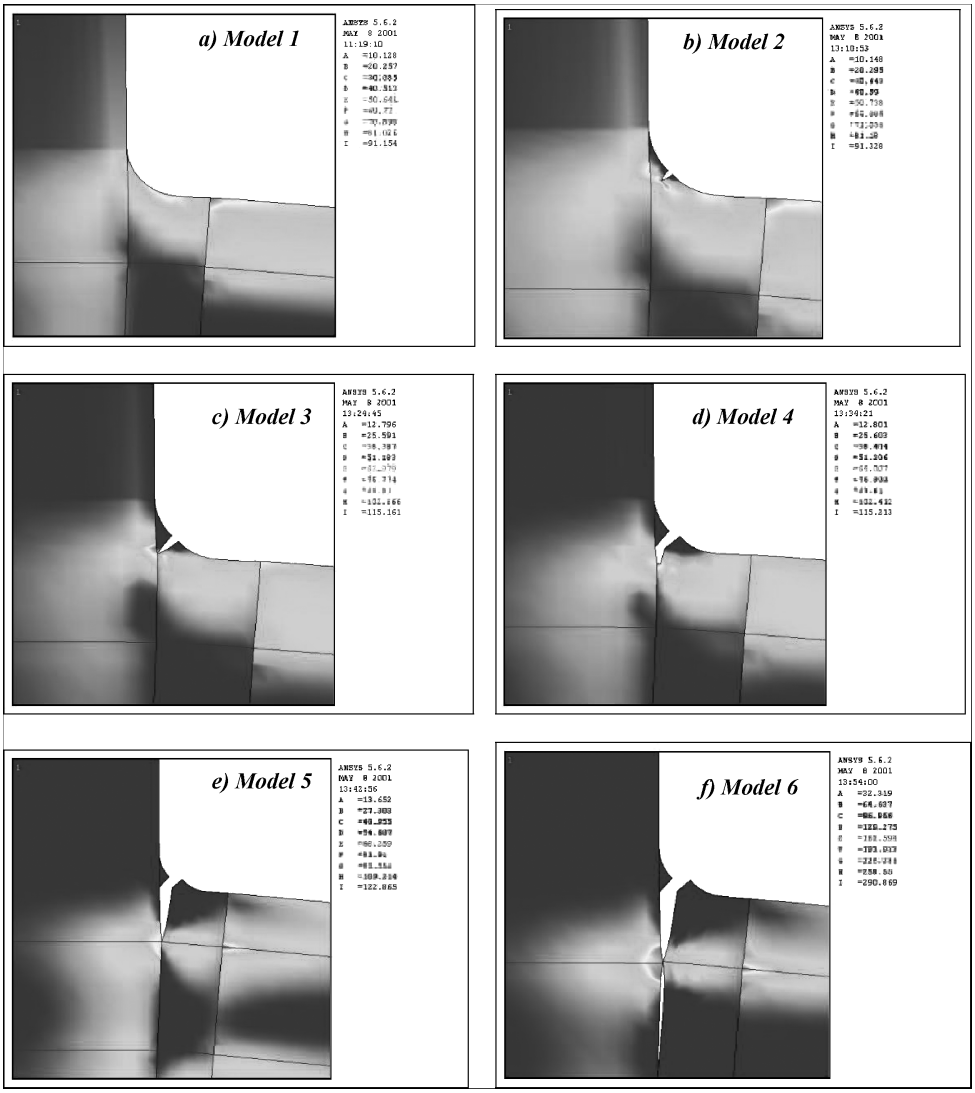

Figure 9. Flexure damage progression effective stress (MPa), σ_{eff}.

loading the fiber insertion adjacent to the applied load in tension and the furthermost fiber insertion in compression. As the fillet matrix stress exceeds the PR520 neat resin tensile strength, a crack initiates at the outer surface of the radius filler. The nonlinear elastic FEA contour plots of Fig. 6 predict that the effective stress in the fillet region will just exceed the matrix tensile stress at the experimentally determined damage-initiation load. Initial T-joint failure may be observed as a discrete drop in the load–displacement record, as shown from point 'a' to 'b' in Fig. 8a. A 25 percent drop in load–displacement at initial damage is typical under

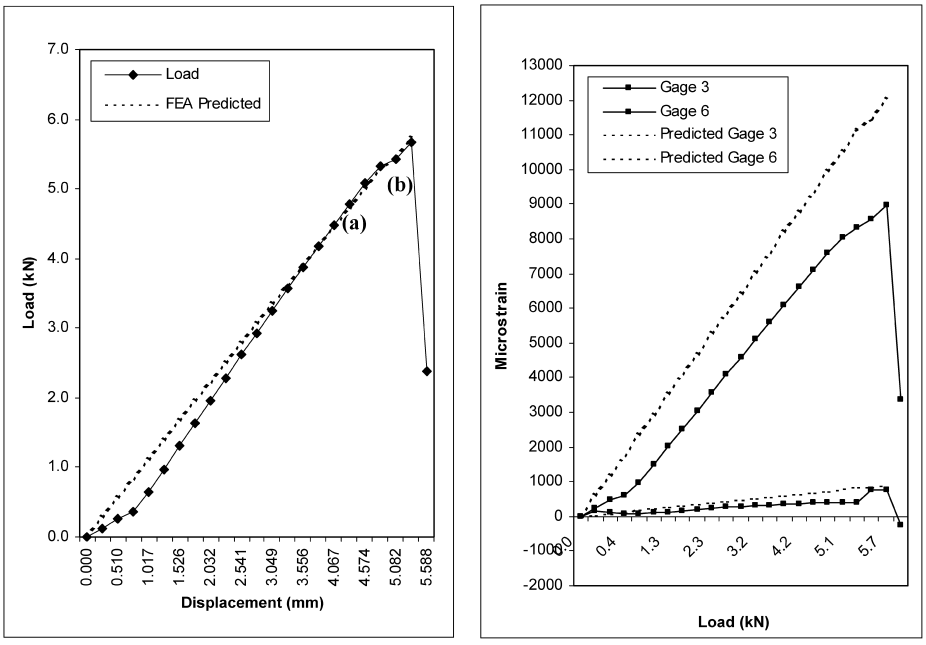

Figure 10. Damage progression under tensile loading: (a) predicted and actual load–displacement and (b) predicted and actual strain–load plot.

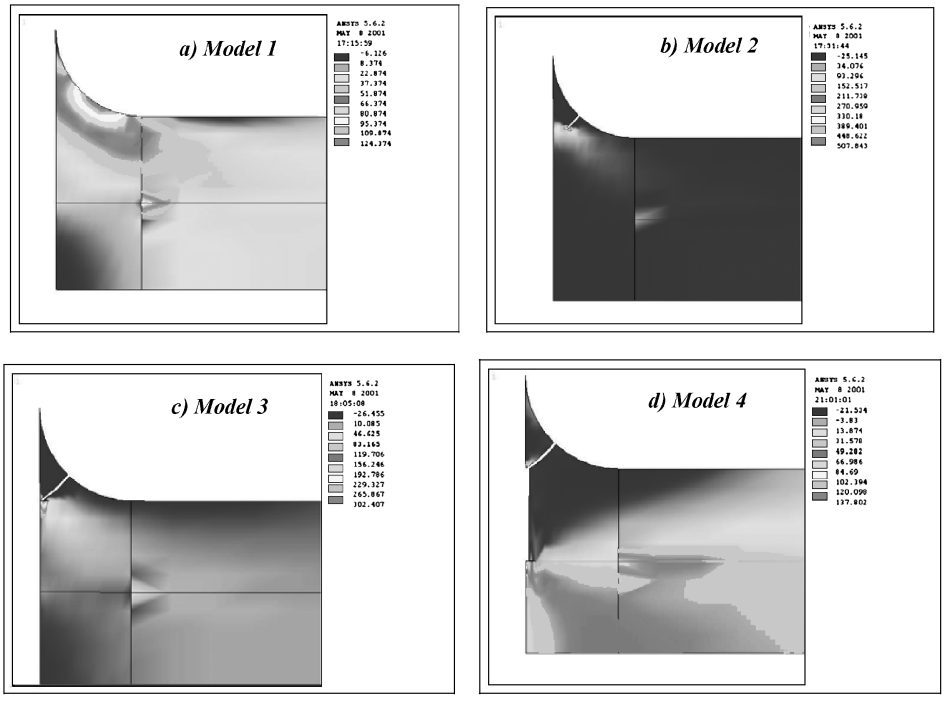

Figure 11. Tensile damage progression normal stress (MPa), σ_x.

flexure loading. The strain–load plot in Fig. 8b shows increased surface strains up to the initial damage load. At the initial damage load, the surface strain–load measurements have a discrete drop in recorded strain, indicating a loss in stiffness of the T-joint under the initial damage.

The extent of initial damage may be characterized by the damage progression FEA. Based on the damage progression models in Fig. 3, it can be shown that in order to match the appropriate response of the T-joint under flexure loading (as shown at points 'a' and 'b' on the load–displacement plot of Fig. 8a, the crack must be extended through the resin-rich fillet region and along the interface to the first fiber insertion. This damage accumulation is represented by the damage progression FEM 5 in Fig. 3e. Good agreement was shown between experimental and predicted results based on the extent of damage represented by model 5 in Fig. 3e.

Region 2 in Fig. 8a is marked by nearly linear load–displacement and strain–load behavior. The initial damage has the effect of redistributing additional load to the first fiber insertion. Increased loading beyond the initial damage load, as represented by region 2 of the load–displacement plot in Fig. 8a point 'b', causes fiber bridging and crack propagation to the neighboring fiber insertion. The fiber bridging behavior gives rise to increased damage tolerance or an ability to carry additional load beyond initial failure. The extent of damage represented by point 'c' of Fig. 8a may be represented by model 6 of the damage progression FEA shown in Fig. 3f. The predicted and actual load–displacement behavior for region 2 is shown in Fig. 8a. Good agreement is shown in region 2 between experimental and predicted results based on the extent of damage represented by model 6 in Fig. 3f.

Region 3 of the load–displacement plot in Fig. 8a from point 'c' to point 'd' is marked by a change in slope and subsequent loss of T-joint stiffness. Under increased load, the fiber insertion adjacent to the applied load continuously degrades. This behavior is represented in the FEA model 6 in Fig. 3f by a change in fiber insertion area. Again, Fig. 5 shows the effect of fiber insertion area on T-joint deflection under flexural loading. As the insertion tow area decreases, the T-joint deflection increases. Based on the use of a fiber-degradation model to represent region 3 in Fig. 8a, good agreement is shown between the experimental and predicted load–displacement behavior.

Figure 12a below, shows the strain–load record for strain gage 1 under flexural loading. Gage 1, as shown in Fig. 12b, is located on the edge of the flexure specimen near the fiber insertion, 0.624 cm from the web-to-flange interface. At initial T-joint failure, a marked jump in strain is shown that may be indicative of load transfer to the fiber insertion after fillet and flange-to-web interface matrix cracking. Also observed is a small jump, followed by a leveling off of the strain in Region 3. This is likely to be due to fiber insertion degradation. The marked reduction in strain at the onset of ultimate failure is likely caused by fiber insertion failure and pullout as shown on the optical micrograph of Fig. 12c. This experimental evidence supports the mechanical behavior presented above.

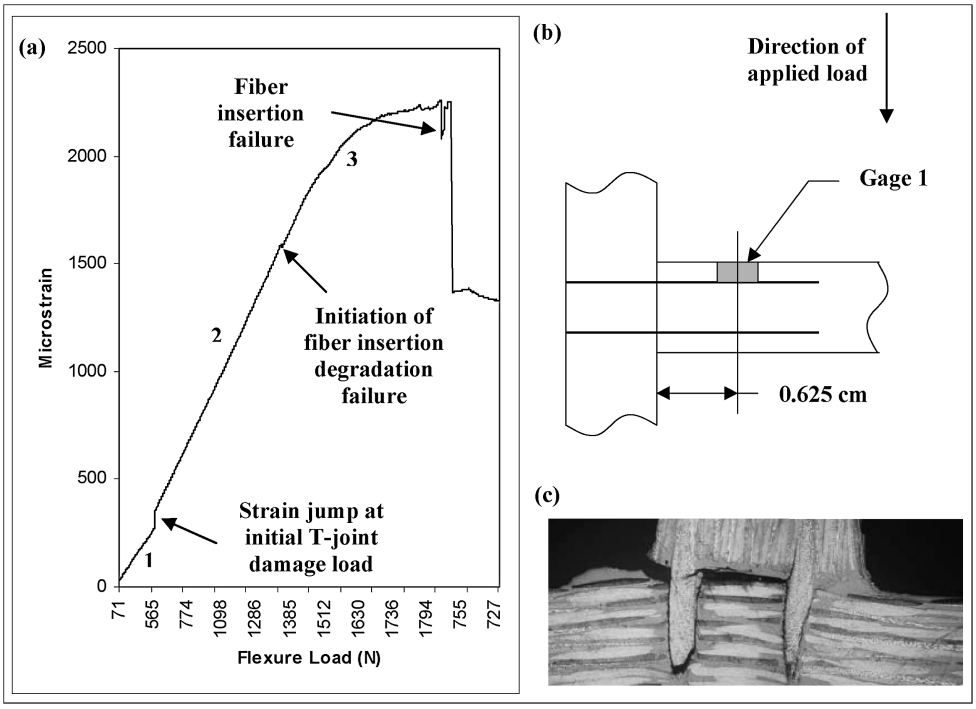

Figure 12. Strain–load record for flexure specimen F1 Gage 1: (a) showing damage accumulation events, (b) local instrumentation layout, and (c) optical micrograph of failed specimen.

5.2. Tension analysis

The mechanical behavior of the T-300/PR520 transverse stitched T-joint under simple support tensile loading is marked by linear elastic behavior up to initial failure and ultimate failure occurring by fiber insertion breakage and pullout. In this case, the fiber insertions are loaded symmetrically in tension. This symmetric loading of the fiber insertions gives the tensile specimens a far greater load carrying capability than that of flexure loading. The initial damage load under simple support tension is approximately ten times greater than that of flexure. The ultimate load carrying capability under tension is approximately three times greater than that of flexure.

The mechanical behavior under tensile loading may be divided into two distinct regions as shown in Fig. 10a. In region 1, the flange deflects elastically under increased load up to point ‘a’ on the load displacement plot. Region 2 is marked by additional linear behavior up to point ‘b’ or ultimate load. The linear elastic finite element analysis of Fig. 10a predicts the behavior in region 1. Good agreement is shown between the experimental and predicted load–displacement. Near the initial damage load, the fillet region at the web-to-flange interface exceeds that of the PR520 neat resin tensile strength. This is also shown in the stress contour plots of Fig. 11. At the damage initiation load, a crack initiates in the fillet region

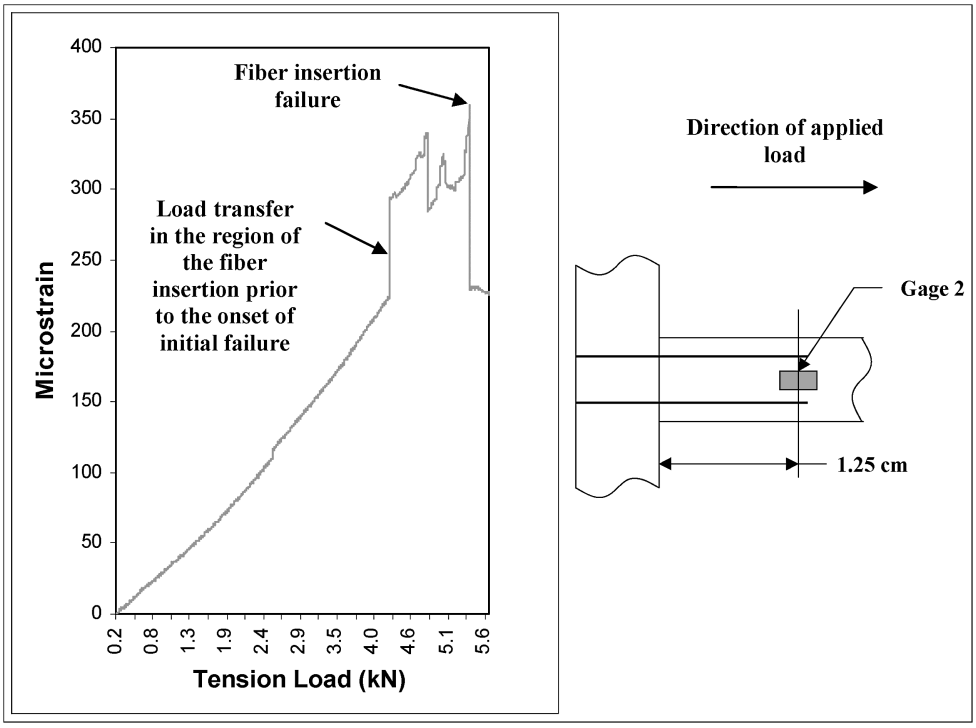

Figure 13. Strain–load record for simple support tension specimen T2 Gage 2: (a) showing damage accumulation events and (b) local instrumentation layout.

and propagates to the fiber insertions. This causes a marked drop in the load–displacement as shown at point 'a' of Fig. 10a. A 3–5% drop in load was noted at initial T-joint failure. A similar response is recorded in the strain–load plot as shown in Fig. 10b.

Based on the optical micrographs of the failed tension specimens, the direction and extent of damage may be determined. In the damage progression finite element model, the crack is initiated when the effective stress exceeds the tensile strength of the matrix. Based on the predicted and actual load–displacement response at initial failure as shown in Fig. 10, the extent of T-joint damage may be determined. The extent of damage that provides a similar response as the experimental load–displacement is represented by Fig. 4c model 3, where the crack is shown starting at the radius fillet and continuing along the web-to-flange interface to the fiber insertions. The damage progression finite element model 3 shows good agreement with the experimental results at point 'a' in Fig. 10a.

Increased loading beyond the initial damage as defined as region 2 of the load–displacement plot of Fig. 10a causes fiber bridging. This fiber bridging gives the T-joint an increased damage tolerance or an ability to carry additional load after first failure occurs. Region 2 of the experimental load–displacement is represented by

model 4 in the damage progression finite element analysis. Again, good agreement is shown between predicted and actual load–displacement in region 2.

Figure 13a shows the strain–load plot for simple support tension strain gage location 2. This gage is located on the edge of the specimen at the maximum depth of the fiber insertion as shown in Fig. 13b. Just prior to the initial damage load, a jump in strain is noted. This jump may be due to increased load transfer to the fiber insertion at the onset of matrix cracking at the web-to-flange interface. Also shown is a discrete drop in strain at T-joint ultimate load that is likely due to fiber insertion failure. Several other discrete events are observed at various stages of damage accumulation.

6. CONCLUSION

A new type of T-joint with transverse stitching using a fiber insertion process was characterized for the first time using linear, nonlinear, and damage progression FEAs. The linear and nonlinear flexure FEAs and the linear elastic tension FEA showed good correlation with experimental results through initial T-joint failure. Crack initiation is predicted under flexure and tension loading when the local matrix stress exceeds that of the neat resin tensile strength in the fillet region of the T-joint. The flexure and tension damage progression FEAs showed good correlation with the experimentally determined load–displacement through ultimate failure. The initial damage load under simple support tension is approximately ten times greater than that of flexure. The ultimate load carrying capability under tension is approximately three times greater than that of flexure. In the case of T-joint flexure loading, the fiber insertions are loaded asymmetrically. Under simple support tension loading, the fiber insertions are loaded symmetrically. The symmetric loading of the fiber insertions gives the tensile specimens a far greater load carrying capability than that of flexure loading. Predictive models developed herein will be used in future parametric studies.

Acknowledgements

The authors would like to acknowledge Albany international Techniweave, Inc., for the development of the fiber insertion process and The Boeing Company for providing funding for this research.

REFERENCES

1. J. W. Gillespie and R. B. Pipes, Behavior of integral composite joints — finite element and experimental evaluation, *J. Compos. Mater.* **12**, 408–421 (1978).
2. L. Tong and L. K. Jain, Analysis of adhesive bonded composite lap joints with transverse stitching, *Appl. Compos. Mater.* **2**, 343–365 (1995).
3. L. Tong and G. P. Steven, A numerical study on stresses in RTM lap joints reinforced with transverse stitching, *Composite Structures* **36**, 91–100 (1996).

4. D. J. Barrett, The mechanics of Z-fiber reinforcement, *Composite Structures* **36**, 23–32 (1996).
5. R. Jones and H. Alesi, On the analysis of composite structures with material and geometric non-linearities, *Composite Structures* **50**, 417–431 (2000).
6. W. K. Chiu, S. Galea and R. Jones, The role of material nonlinearities in composite structures, *Composite Structures* **38**, 71–81 (1997).
7. H. J. Phillips and R. A. Shenoi, Damage tolerance of laminated tee joints in FRP structures, *Composites Part A* **29**, 465–478 (1998).
8. J. I. R. Blake, R. A. Shenoi, J. House and T. Turton, Progressive damage analysis of tee joints with viscoelastic inserts, *Composites Part A* **32**, 641–653 (2001).
9. P. B. Stickler, An investigation of mechanical behavior and failure mechanisms of composite T-joints with transverse stitching, PhD Dissertation, University of Washington (2001).
10. P. B. Stickler, M. Ramulu and P. S. Johnson, Experimental and numerical analysis of transverse stitched T-joints in bending, *Composite Structures* **50**, 17–27 (2000).
11. P. B. Stickler, M. Ramulu and B. Van West, Transverse stitched T-joints in bending with PR520 resin: initial results, *J. Reinforced Plast. Compos.* **20**, 65–75 (2001).
12. P. B. Stickler and M. Ramulu, Investigation of mechanical behavior of transverse stitched T-joints with PR520 resin in flexure and tension, *Composite Structures* **52**, 307–314 (2001).
13. ANSYS, Inc. Version 5.6 Users Manual, Canonsburge, PA (2000).
14. IM7 Carbon Fiber Product Data Sheet, Hexcel Carbon Fibers (2001).
15. PR520 Epoxy Resin Product Data Sheet, 3M Corporation (2000).
16. P. B. Stickler, M. Ramulu, S. L. Coguill and M. E. Tuttle, Experimental investigation of T-300/PR520 laminate properties and failure analysis, *J. Adv. Mater*. **36**, 3–11 (2003).
17. B. N. Cox and G. Flanagan, *Handbook of Analytical Methods for Textile Composites.* NASA Contractor Report 4750 (1997).